

Interaction-dominated transport in two-dimensional conductors: From degenerate to partially degenerate regime

G. M. Gusev ¹, A. D. Levin,¹ E. B. Olshanetsky ^{2,3}, Z. D. Kvon,^{2,3} V. M. Kovalev,^{2,4,5}
M. V. Entin,^{2,3} and N. N. Mikhailov ^{2,3}

¹*Instituto de Física da Universidade de São Paulo, 135960-170 São Paulo, SP, Brazil*

²*Institute of Semiconductor Physics, Novosibirsk 630090, Russia*

³*Novosibirsk State University, Novosibirsk 630090, Russia*

⁴*Novosibirsk State Technical University, Novosibirsk 630073, Russia*

⁵*Abrikosov Center for Theoretical Physics, Moscow Institute of Physics and Technology, Dolgoprudny 141701, Russia*



(Received 10 October 2023; revised 8 December 2023; accepted 15 December 2023; published 2 January 2024)

In this study, we investigate the conductivity of a two-dimensional (2D) system in HgTe quantum well comprising two types of carriers with linear and quadratic spectra, respectively. The interactions between the two-dimensional Dirac holes and the heavy holes lead to the breakdown of Galilean invariance, resulting in interaction-limited resistivity. Our exploration of the transport properties spans from low temperatures, where both subsystems are fully degenerate, to higher temperatures, where the Dirac holes remain degenerate while the heavy holes follow Boltzmann statistics, creating a partially degenerate regime. Through a developed theory, we successfully predict the behavior of resistivity as $\rho \sim T^2$ and $\rho \sim T^3$ for the fully degenerate and partially degenerate regimes, respectively, which is in reasonable agreement with experimental observations. Notably, at elevated temperatures, the interaction-limited resistivity surpasses the resistivity caused by impurity scattering by a factor of 5–6. These findings imply that the investigated system serves as a versatile experimental platform for exploring various interaction-limited transport regimes in two component plasma.

DOI: [10.1103/PhysRevB.109.035302](https://doi.org/10.1103/PhysRevB.109.035302)

I. INTRODUCTION

Recent advances in the fabrication of ultra clean two-dimensional (2D) semiconductor systems make it possible to explore the regime, where the interparticle collisions dominate over the impurity and phonon scattering. However, in conventional systems with a parabolic spectrum, where the Umklapp scattering is prohibited or ineffective due to small Fermi surface, the particle-particle scattering does not contribute to the conductivity because it does not change the net current. The situation is changed in systems with a constrained geometry, where electron transport can be described by the laws of hydrodynamics. In this case the electron velocity profile resembles a Poiseuille-like (parabolic) profile and the transport is governed by electron-electron interactions [1–3]. As it was found in the pioneering theoretical study by Gurzhi [1], in this regime the particle-particle collisions manifest themselves as a contribution to resistivity $\sim T^{-2}$, which, however, is essentially impossible to observe in conventional 2D system where electron-phonon and electron-impurity collisions are the dominant scattering mechanisms. Manifestation of Gurzhi effect can be found in GaAs [4–8] and in graphene [9] systems.

Another important 2D system where particle-particle interaction contributes to the conductivity is the degenerate and/or nondegenerate electron-hole (e-h) plasma in semimetals. In general, a system with a simple parabolic spectrum is a Galilean invariant electron liquid, while, as expected, a system with two types of charge carriers that differ in sign and/or effective mass lacks the Galilean invariance [10–12].

Indeed in non-Galilean-invariant liquids the colliding carriers have either opposite charge sign or different spectra, so the net current is not proportional to the total momentum of particles. The strong mutual friction between electrons and holes in a degenerate 2D semimetal leads to the resistivity $\sim T^2$, which has been observed in HgTe quantum wells (QWs) [13,14]. The nondegenerate limit has been explored in a single-layer and bilayer graphene, where e-h pairs are thermally excited [15,16]. The electron-hole collisions rate is expected to be proportional to T , which leads to temperature-independent conductivity. Electron-hole friction regime leading to T^2 resistivity has been explored recently in graphene bilayer with spatially separated electrons and holes [17].

An interesting and important physics is expected to take place when plasma is partially degenerate: Electrons are distributed according to the Fermi statistics, while the ions obey the Boltzmann statistics [18]. The physics associated with the hydrodynamics in a partially degenerate regime has not been explored yet.

In this paper, we present the gapless HgTe quantum well as a versatile platform that hosts two subbands with significantly distinct effective masses. HgTe-based devices offer an exceptional opportunity for investigating transitions between various regimes, as they can be precisely adjusted using gate voltage to control density and system degeneracy.

The HgTe quantum well spectrum depends strongly on the well width [19–21]. At the critical well width $d_c = 6.3–6.5$ nm (depending on the surface orientation and the quantum well deformation), the band gap becomes zero. The HgTe

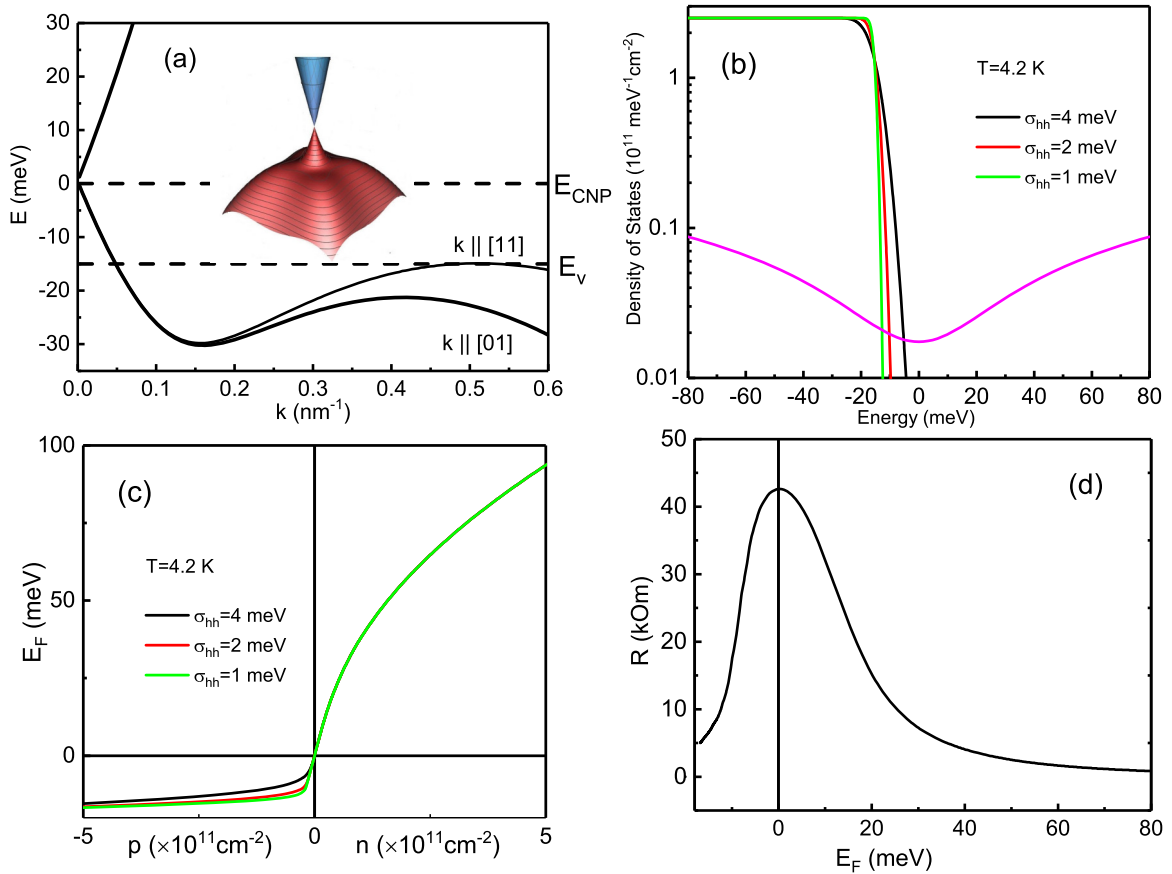


FIG. 1. (a) Schematic representation of the energy spectrum of a 6.4-nm mercury telluride quantum well. Insert demonstrates schematic 3D presentation of the spectrum. (b) Density of the states of the Dirac carriers (magenta) and heavy holes for different values of the heavy hole broadening parameter σ_{hh} . (c) The Fermi energy as a function of the charge carriers density. (d) The resistance of the 6.4 nm sample as a function of the Fermi energy for $\sigma_{hh} = 2 \text{ meV}$ at $T = 4 \text{ K}$.

QWs with the width larger than d_c are the two-dimensional (2D) topological insulator [22,23] and 2D semimetal [13,14].

The energy spectrum of a gapless HgTe quantum well with the width of 6.3–6.5 nm consists of a single valley Dirac cone leading to some unusual electron transport properties [24–29]. At the same time, besides the Dirac-like holes in the center of the Brillouin zone, the valence band has lateral heavy hole valleys located some distance below the Dirac point [Fig. 1(a)]. It may be expected that the coexistence of the 2D Dirac-like holes and the heavy holes at a finite wave vector k will result in the resistance increasing with temperature since the low-mobility heavy holes will change the electron momentum during collisions. Therefore the gapless HgTe well allows us to study the scattering between the conventional and the Dirac particles.

In the present paper we report the experimental and theoretical study of the transport in a gapless HgTe quantum well with the width of $d_c = 6.3$ –6.5 nm. In the region where the holes with the linear and the parabolic spectrum coexist, the system lacks the Galilean invariance and we observe resistivity $\rho \sim T^2$ in the fully degenerate and $\rho \sim T^\alpha$ ($\alpha \approx 3$) in the partially degenerate regimes, where the heavy holes obey the Boltzmann statistic, while the Dirac holes remain degenerate. Such T dependence is attributed to the mutual friction between the Dirac and the heavy holes.

II. ELECTRON SPECTRUM IN A GAPLESS HgTe-BASED QUANTUM WELL

To understand the transport properties of the charge carriers in a gapless HgTe quantum well we first show the energy spectrum in a wide energy interval for both conductance and the valence bands in Fig. 1(a). Such HgTe well hosts the Dirac fermions with a linear electron and holes spectrum $\varepsilon_e = \pm v|k|$, where the Fermi velocity is $v = 7 \times 10^7 \text{ cm/s} = c/430$ (c is the light velocity) and k is the momentum. In addition one can see the lateral maximum of the valence band below the charge neutrality point: k_0 is defined as $vk_0 = \mu$, $p_0 = m_h v_F = \sqrt{2m_h(\mu - \Delta)}$, v_F is the Fermi velocity of the heavy holes, $m_h = 0.15m_0$ is the effective mass of the holes, μ is the electrochemical potential, and $\Delta \approx 15 \text{ meV}$, where $\Delta = |E_v - E_{CNP}|$. The band structure has been computed in various previous studies [24,27]. Specifically, we employed the model outlined in our earlier paper [30], where comprehensive details of the calculations were provided. Figures 1(b) and 1(c) show the density of states (DOS) for Dirac carriers and heavy holes and the Fermi energy at $T = 4.2 \text{ K}$ respectively for different heavy hole broadening parameter σ_{hh} . Because of the large effective mass and the valley degeneracy

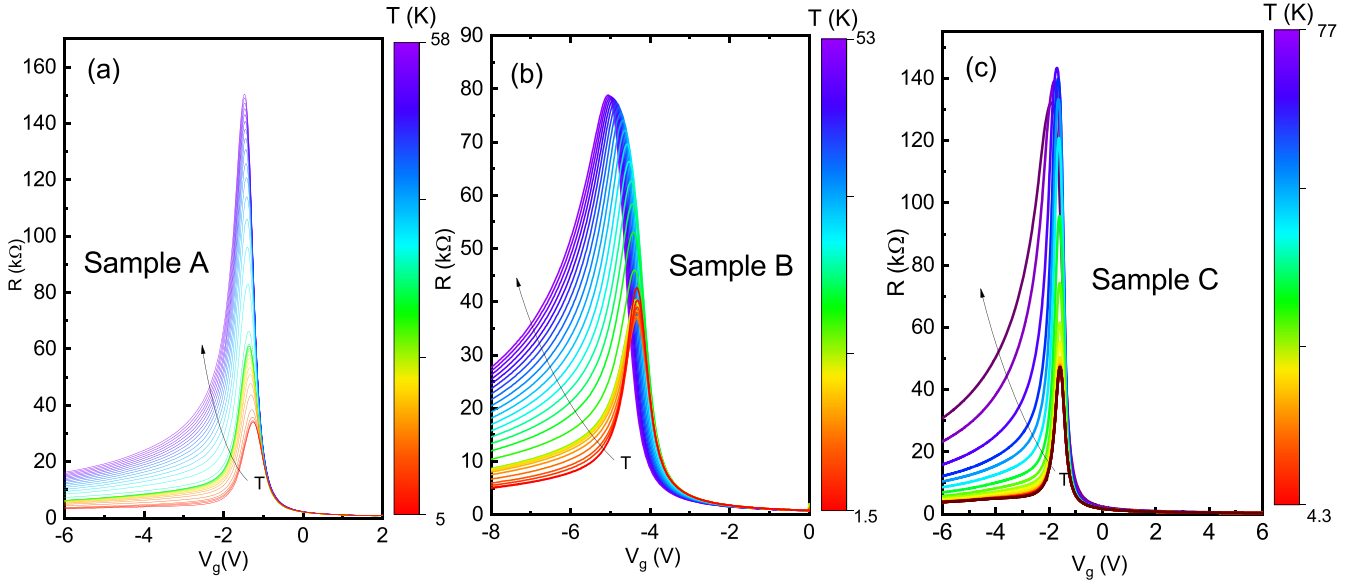


FIG. 2. Resistance as a function of the gate voltage at different temperatures for three HgTe gapless quantum wells, $d = 6.4$ nm, device A (a); $d = 6.3$ nm, device B (b); and $d = 6.4$ nm, device C (c).

$g_v = 2$ the density of states of the heavy holes (HH) is much larger than the density of states of the Dirac holes (DH). In realistic samples the in-plane fluctuations of the QW width about its average value $d \approx d_c$, that cannot be avoided during the QW growth, lead to in-plane variations of the bands gap [31], and, consequently, to variations of the charge neutrality point (CNP) and E_v positions. This results in a broadening of the density of states as shown in Fig. 1(b). From topological network model, described in Ref. [31] we estimate the DOS broadening $\sim 1-4$ meV. The Fermi energy pinning in the tail of the heavy-hole DOS [Fig. 1(c)] may lead to a strong asymmetry of the $R(V_g)$ dependence in contrast to graphene. Figure 1(d) demonstrates the resistance as a function of the Fermi energy for one of the typical gapless HgTe QW sample. The Fermi level crosses E_v for parameters $\sigma_{hh} = 1-4$ meV. For large broadening $\sigma_{hh} = 6$ meV the Fermi level does not cross E_v because it gets pinned in the disorder induced heavy holes DOS tail [Fig. 1(c)] and the Dirac holes move through isolated islands or puddles where HH and DH coexist. Below for simplicity we consider a homogeneous two-component conductance model.

III. SAMPLE DESCRIPTION AND METHODS

We have measured the resistance of quantum wells $\text{Cd}_{0.65}\text{Hg}_{0.35}\text{Te}/\text{HgTe}/\text{Cd}_{0.65}\text{Hg}_{0.35}\text{Te}$ with (013) surface orientations and the well width of 6.3–6.5 nm. The samples were grown by means of molecular beam epitaxy at $T \approx 160-200^\circ\text{C}$ on GaAs substrate with the (013) surface orientation [32]. Such inclined to 100 orientation substrates have been used in order to increase the quality of the material. Layer sequence scheme and details of the sample preparation have been published previously. The experimental devices were Hall bars with eight voltage probes divided into three

separate segments with the width W of $50 \mu\text{m}$ and the lengths L (100, 250, $100 \mu\text{m}$) between the probes. A dielectric layer (200 nm of SiO_2) was deposited on the sample surface followed by a TiAu gate electrode. Ohmic contacts to the quantum well has been fabricated by annealing of indium on the device contact pads. The sheet density variation with gate voltage was $1.1 \times 10^{11} \text{ cm}^{-2} \text{ V}^{-1}$. Because of the dielectric breakdown the limiting gate voltage was $\pm 8 \text{ V}$. The measurements of the resistance $R(T)$ has been performed in the temperature range 4.2–70 K using a conventional four-probe set up with a 1–27 Hz ac current of 1–10 nA through the sample.

IV. EXPERIMENTAL RESULTS

Figure 2 presents the resistance as a function of the gate voltage obtained over a wider temperature range for three different samples A, B, and C. Table I lists the typical parameters of the gapless HgTe quantum well, used in this study, such as the well width d , the gate voltage corresponding to the Dirac point position V_{CNP} , the resistivity (ρ value at the CNP) and the electron mobility $\mu_e = 1/\rho n_s$ for the electron density $n_s = 10^{11} \text{ cm}^{-2}$. The evolution of the resistance with temperature is similar in all samples: at the hole side of the energy spectrum the resistance increases with T, indicating a metallic type of conductivity. Moreover, with T increasing the resistance peak shifts to the hole side and becomes wider,

TABLE I. Some of the typical parameters of the electron system in HgTe quantum well at $T = 4.2$ K.

Sample	d (nm)	V_{CNP} (V)	$\rho_{\text{max}}(h/e^2)$	$\mu_e \mu_e$ ($\text{V}/\text{cm}^2\text{s}$)
A	6.4	-1.3	0.26	96.000
B	6.3	-4.3	0.33	63.000
C	6.4	-1.6	0.37	105.600

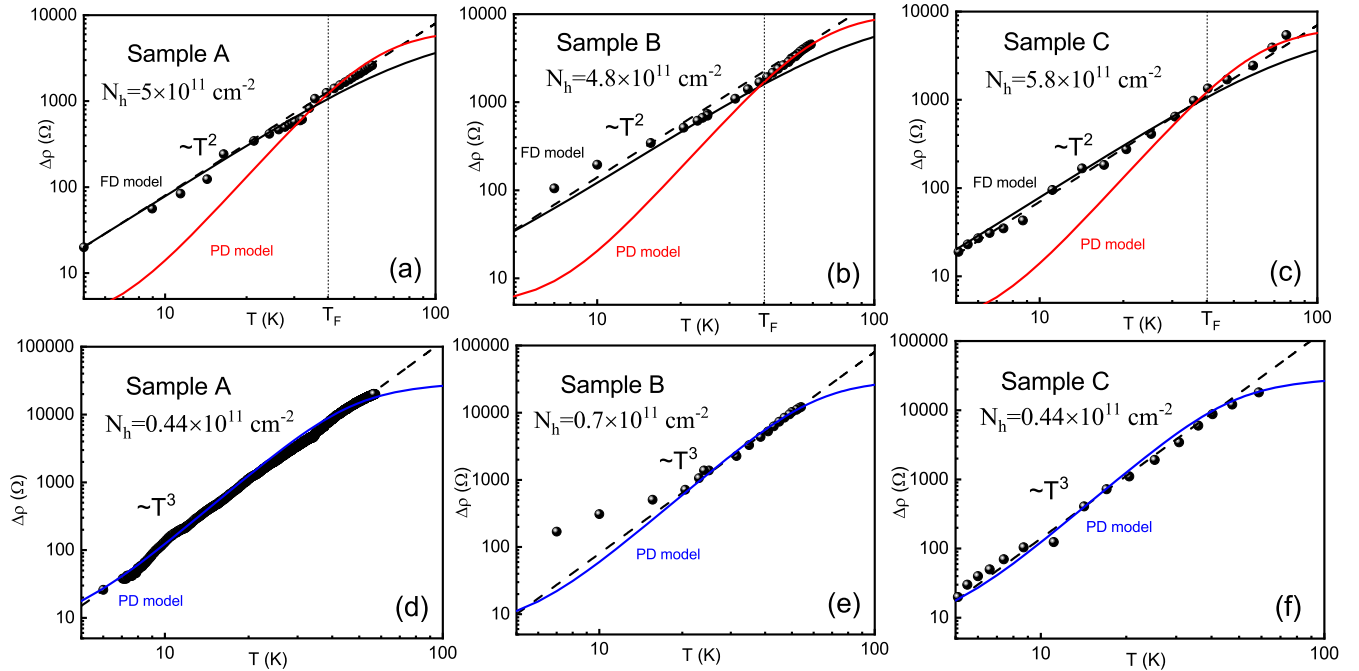


FIG. 3. Excess resistivity $\Delta\rho(T) = \rho(T) - \rho(T = 4.2 \text{ K})$ as a function of the temperature for high [(a),(b),(c)] and low [(d),(e),(f)] densities for three HgTe quantum wells. (a) The total density is $N_h = 5 \times 10^{11} \text{ cm}^{-2}$ (sample A); (b) $4.8 \times 10^{11} \text{ cm}^{-2}$ (sample B); and (c) $5.8 \times 10^{11} \text{ cm}^{-2}$ (sample C). Vertical line indicates T_F Fermi temperature of the heavy holes. (d) The total density is $N_h = 0.44 \times 10^{11} \text{ cm}^{-2}$ (sample A); (e) $0.7 \times 10^{11} \text{ cm}^{-2}$ (sample B); and (f) $0.44 \times 10^{11} \text{ cm}^{-2}$ (sample C). Circles represent the experimental data, the blue lines represent the theory of interparticle scattering between the fully degenerate particles (FD model), the red lines represent the theory of interparticle scattering between fully the degenerate Dirac holes nondegenerate heavy holes (PD model), dashes represents T^2 (a), (b), (c) and T^3 (d), (e), (f) dependencies.

while the resistance at the electronic side remains temperature independent.

In order to analyze the functional form of the resistance (resistivity) dependence, it could be instructive to subtract T -independent contribution to $\rho(T)$ and calculate the excess resistivity $\Delta\rho(T) = \rho(T) - \rho(T = 4.2 \text{ K})$. We plot the experimentally measured excess resistivity $\Delta\rho(T)$ as a function of temperature for all three devices and at the highest negative gate voltages in Figs. 3(a)–3(c). One can see that $\Delta\rho(T)$ exhibits peculiar T^2 growth, varying by almost two orders of magnitude. At temperatures $T > 20$ –30 K, $\Delta\rho(T)$ reveals a cubic rather than quadratic temperature dependence. A stronger T dependence at high temperatures is related to the transition from the fully degenerate to a partially degenerate regime, where the heavy holes obey the Boltzmann statistic. At the highest negative gate voltage we achieve the chemical potential $\mu - \Delta \approx 2 \text{ meV}$ with corresponding Fermi temperature $T_F = (\mu - \Delta)/k \approx 30 \text{ K}$ [see Fig. 3(a)], while the chemical potential μ is $\mu \approx 17 \text{ meV}$, k is the Boltzmann constant. Figures 3(d)–3(f) show the $\Delta\rho(T)$ dependencies at a low total carrier density, where the partially degenerate regime is expected over the whole temperature interval. One can see that the experimental data closely follows $\Delta\rho(T) \sim T^3$ dependence.

The peculiar T^2 and T^3 resistance dependencies are the signature of a particle-particle scattering, because the scattering by phonons would result in a linear rather than quadratic T dependence [33]. While it is well known that the electron-electron interaction cannot affect the resistivity of a

Galilean-invariant Fermi liquid, there are situations where a conductivity $\sim T^{-2}$ [34] may be observed, such as a multiply connected Fermi surface [34], the presence of spin-orbit interaction [11], or several subbands [12,34–37].

In concluding this section we would like to discuss the potential impact of temperature on the band structure of HgTe quantum wells [38–40]. Notably, this impact becomes more apparent at elevated temperatures beyond 70 K. The manifestation of the quantum Hall effect and Shubnikov-de Haas (SdH) oscillations in HgTe wells at $T > 70 \text{ K}$ suggests a limited sensitivity of transport properties to higher temperatures [41,42]. Neither the Shubnikov-de Haas oscillations nor the Hall effect undergo significant changes at $T < 70 \text{ K}$. It is noteworthy that we exclusively observed T^2 and T^3 dependencies for hole contributions to resistivity, with no corresponding dependencies for electrons. Emphasizing the importance of band gap opening, we expect an activation-type temperature dependence of resistivity, consistent with our observations in samples with an 8-nm well width exhibiting a gap [23]. The diverse experiments carried out by various research groups, coupled with recent theoretical calculations [43], indicate that providing a definitive demonstration of a significant temperature impact on the gap in HgTe wells below 70 K remains elusive. Furthermore, the presence of the gap leads to an opposite temperature dependence of resistance, wherein resistance typically decreases with increasing temperature. In contrast, our observations in the sample indicate an increase in resistance with rising temperature (Fig. 2) [23,30].

V. TWO-SUBBAND HYDRODYNAMIC MODEL

Below we consider a simple two-subband hydrodynamic model, where the hole-hole scattering is described in terms of a mutual friction. The conductivity can be found from the equation of motion for the holes with Dirac dispersion and the heavy holes,

$$-\frac{v_d - v_h}{\tau_{dh}} - \frac{v_d}{\tau_d} + \frac{qE}{m_d} = 0; \quad -\frac{v_h - v_d}{\tau_{hd}} - \frac{v_h}{\tau_h} + \frac{qE}{m_h} = 0; \quad (1)$$

$$v_d = \frac{Eq\tau_d(m_d\tau_h\tau_{hd} + \tau_{dh}m_h(\tau_h + \tau_{hd}))}{m_d m_h(\tau_d\tau_{hd} + \tau_{dh}(\tau_h + \tau_{hd}))};$$

$$v_h = \frac{Eq\tau_h(\tau_d\tau_{dh}m_h + m_d\tau_{hd}(\tau_d + \tau_{dh}))}{m_d m_h(\tau_d\tau_{hd} + \tau_{dh}(\tau_h + \tau_{hd}))}; \quad (2)$$

where E is the electric field, $v_{h,d}$ are the carrier velocities for heavy (h) and Dirac (d) holes, m_h is heavy hole effective mass, $m_d = \mu/v^2$ is Dirac hole effective mass, $\tau_{h(d)}$ are the momentum relaxation times, and $\tau_{hd(dh)}$ is collision time with heavy (Dirac) holes per Dirac (heavy) holes,

$$\tau_{dh} = \frac{\tau_{\text{int}}(m_d n_d + m_h n_h)}{m_h n_h}, \quad \tau_{hd} = \frac{\tau_{\text{int}}(m_d n_d + m_h n_h)}{m_d n_d}. \quad (3)$$

$$j = \left[\frac{q^2(n_d + n_h)(n_d\tau_d(\tau_h + \tau_{\text{int}}) + n_h\tau_h(\tau_d + \tau_{\text{int}}))}{m_h n_h(\tau_d + \tau_{\text{int}}) + m_d n_d(\tau_h + \tau_{\text{int}})} \right] E - \left[\frac{q^2 n_d n_h \tau_{\text{int}}(m_d + m_h)(m_d\tau_h - \tau_d m_h)}{m_d m_h(m_h n_h(\tau_d + \tau_{\text{int}}) + m_d n_d(\tau_h + \tau_{\text{int}}))} \right] E, \quad (8)$$

$$\sigma = q^2 \frac{n_d n_h \left[\tau_d(\tau_h + \tau_{\text{int}}) \left(2 + \frac{n_d}{n_h} \right) + \tau_h(\tau_d + \tau_{\text{int}}) \frac{n_h}{n_d} + \tau_{\text{int}} \left(\frac{m_h}{m_d} \tau_d - \frac{m_d}{m_h} \tau_h \right) \right]}{m_h n_h(\tau_d + \tau_{\text{int}}) + m_d n_d(\tau_h + \tau_{\text{int}})}, \quad (9)$$

where we used the expression for the conductivity $j = \sigma E$.

One might anticipate that the scattering times $\tau_{d(h)}$ associated with impurity and interface roughness scattering remain temperature independent. On the other hand, the scattering time τ_{int} attributed to hole-hole friction is accountable for the temperature-dependent contribution to conductivity in the non-Galilean hole liquid.

It would be instructive to consider $T = 0$ and $T = \infty$ limits in the case when the effective masses are significantly different. The Dirac hole effective scattering time can be estimated from relation $m_d = \mu/v^2 \approx 0.006m_0$, at $\mu \approx 16$ meV.

At $T \rightarrow 0$ both bands contribute to the total conductivity dominated by Dirac holes,

$$\sigma(T = 0) = \frac{q^2 n_d v^2 \tau_d}{\mu} = \frac{q^2 n_d \tau_d}{m_d}. \quad (10)$$

At $T = \infty$ the conductivity becomes temperature independent and saturates at a value approximately determined by the conductivity of the heavy hole band,

$$\sigma(T = \infty) = \frac{q^2(n_d + n_h)^2 \tau_h}{m_h n_h}. \quad (11)$$

The ratio of the resistivities at both temperature limits is given by

$$\frac{\rho(T = \infty)}{\rho(T = 0)} = \frac{m_h n_h n_d \tau_d}{m_d(n_d + n_h)^2 \tau_h}. \quad (12)$$

One can introduce the center-of-mass velocity and the relative velocity,

$$U = \frac{m_d n_d v_d + m_h n_h v_h}{m_d n_d + m_h n_h}, \quad V = v_d - v_h. \quad (4)$$

Resolving Eqs. (1)–(4) we obtain

$$U = \frac{qE(n_h\tau_h(\tau_d + \tau_{\text{int}}) + n_d\tau_d(\tau_h + \tau_{\text{int}}))}{m_h n_h(\tau_d + \tau_{\text{int}}) + m_d n_d(\tau_h + \tau_{\text{int}})}, \quad (5)$$

$$V = \frac{qE(m_d n_d + m_h n_h)(\tau_d m_h - m_d \tau_h)}{m_d m_h(m_h n_h(\tau_d + \tau_{\text{int}}) + m_d n_d(\tau_h + \tau_{\text{int}}))} \tau_{\text{int}}, \quad (6)$$

where $1/\tau_{\text{int}} = 1/\tau_{dh} + 1/\tau_{hd}$. This equation considering the constraint that interactions between holes conserve the overall momentum density: $n_d m_d \tau_{dh} = n_h m_h \tau_{hd}$. The initial term signifies the impact arising from the movement of the Dirac and heavy holes in opposing directions due to the contrasting forces imposed on them by the electric field. On the other hand, the second term indicates the influence resulting from Dirac and heavy holes collectively moving in the same direction due to the Coulomb drag, analogous to a ‘‘friction,’’ occurring between them,

$$j = (n_d + n_h)qU + \frac{n_d n_h}{m_d n_d + m_h n_h} (m_d + m_h)qV, \quad (7)$$

In our case $n_h \gg n_d$, the ratio of the resistivities at both temperature limits is determined by

$$\frac{\rho(T = \infty)}{\rho(T = 0)} = \frac{m_h n_d \tau_d}{m_d n_h \tau_h}. \quad (13)$$

It is important to consider the resistivity at the two opposite temperature limits. If $n_d \tau_d \sim n_h \tau_h$ the ratio of the resistivities corresponding to the two temperature limits is determined by the effective mass ratio $\frac{\rho(T=\infty)}{\rho(T=0)} \approx \frac{m_h}{m_d} \approx 50$.

Thus, impurity scattering is predominant at lower temperatures, while the hole-hole interaction dominates at higher temperatures. Here, one can highlight, as evident from Fig. 2, that in actual samples, the hydrodynamic conductivity can surpass the Drude conductivity by a factor of 5 to 6. This observation underscores that our system stands out as a liquid with the highest hydrodynamic conductivity when compared to other systems, as discussed in Refs. [2] and [3]. Consequently, it serves as a promising platform for investigating various hydrodynamic phenomena, such as the violation of the Wiedemann-Franz law, collective sound modes, and non-linear behaviors (refer to [2] and [3] for a comprehensive review).

In the next section we consider theoretically mechanism of the scattering between Dirac and heavy holes.

VI. CALCULATION OF THE SCATTERING TIME. DEGENERATE DIRAC AND PARABOLIC (HEAVY) HOLES

The formula $\epsilon_{\mathbf{k}} = v\mathbf{k}$ represents the energy of Dirac particles, \mathbf{k} is the momentum, v is velocity. The formula for particles with parabolic spectrum is $\epsilon_{\mathbf{p}} = p^2/2m + \Delta$, where \mathbf{p} is the heavy hole momentum, $m = m_h$ is the heavy hole mass. Let us set the Planck and Boltzmann constants to be 1 for the calculations, and in the final equations, we will revert to its original value. The kinetic equation for Dirac particles is given by

$$(\mathbf{F}, \mathbf{v}_{\mathbf{k}}) \frac{\partial n_{\mathbf{k}}}{\partial \epsilon_{\mathbf{k}}} = 2\pi \sum_{\mathbf{p}', \mathbf{k}', \mathbf{p}} |U_{\mathbf{p}'-\mathbf{p}}|^2 [(1-f_{\mathbf{k}})(1-f_{\mathbf{p}})f_{\mathbf{k}'}f_{\mathbf{p}'} - (1-f_{\mathbf{k}'})(1-f_{\mathbf{p}'})f_{\mathbf{k}}f_{\mathbf{p}}] \times \delta(\epsilon_{\mathbf{k}'} + \epsilon_{\mathbf{p}'} - \epsilon_{\mathbf{k}} - \epsilon_{\mathbf{p}}) \delta_{\mathbf{k}'+\mathbf{p}'-\mathbf{k}-\mathbf{p}}. \quad (14)$$

For heavy hole particles with parabolic spectrum the kinetic equations is

$$(\mathbf{F}, \mathbf{v}_{\mathbf{p}}) \frac{\partial n_{\mathbf{p}}}{\partial \epsilon_{\mathbf{p}}} = 2\pi \sum_{\mathbf{p}', \mathbf{k}', \mathbf{k}} |U_{\mathbf{p}'-\mathbf{p}}|^2 [(1-f_{\mathbf{k}})(1-f_{\mathbf{p}})f_{\mathbf{k}'}f_{\mathbf{p}'} - (1-f_{\mathbf{k}'})(1-f_{\mathbf{p}'})f_{\mathbf{k}}f_{\mathbf{p}}] \times \delta(\epsilon_{\mathbf{k}'} + \epsilon_{\mathbf{p}'} - \epsilon_{\mathbf{k}} - \epsilon_{\mathbf{p}}) \delta_{\mathbf{k}'+\mathbf{p}'-\mathbf{k}-\mathbf{p}}. \quad (15)$$

Here $\mathbf{v}_{\mathbf{k}} = v\mathbf{k}/k$ and $\mathbf{v}_{\mathbf{p}} = \mathbf{p}/m$ are velocity of the Dirac and parabolic holes, consequently. We will linearize these equations with small corrections to the distribution functions $f_{\mathbf{k}} = n_{\mathbf{k}} + \delta f_{\mathbf{k}}$ and $f_{\mathbf{p}} = n_{\mathbf{p}} + \delta f_{\mathbf{p}}$, where $n_{\mathbf{k}}$ and $n_{\mathbf{p}}$ represents equilibrium distributions of Dirac and parabolic holes.

Assuming that in the kinetic equation for Dirac holes, the parabolic holes are in equilibrium (and vice versa), we obtain

$$(\mathbf{F}, \mathbf{v}_{\mathbf{k}}) \frac{\partial n_{\mathbf{k}}}{\partial \epsilon_{\mathbf{k}}} = -2\pi \sum_{\mathbf{p}', \mathbf{k}', \mathbf{p}} |U_{\mathbf{p}'-\mathbf{p}}|^2 [\delta f_{\mathbf{k}} [(1-n_{\mathbf{p}})n_{\mathbf{k}'}n_{\mathbf{p}'} + n_{\mathbf{p}}(1-n_{\mathbf{k}'})(1-n_{\mathbf{p}'})] - \delta f_{\mathbf{k}'} [(1-n_{\mathbf{k}})(1-n_{\mathbf{p}})n_{\mathbf{p}'} + n_{\mathbf{k}}n_{\mathbf{p}}(1-n_{\mathbf{p}'})]] \times \delta(\epsilon_{\mathbf{k}'} + \epsilon_{\mathbf{p}'} - \epsilon_{\mathbf{k}} - \epsilon_{\mathbf{p}}) \delta_{\mathbf{k}'+\mathbf{p}'-\mathbf{k}-\mathbf{p}}, \quad (16)$$

$$(\mathbf{F}, \mathbf{v}_{\mathbf{p}}) \frac{\partial n_{\mathbf{p}}}{\partial \epsilon_{\mathbf{p}}} = -2\pi \sum_{\mathbf{p}', \mathbf{k}', \mathbf{k}} |U_{\mathbf{p}'-\mathbf{p}}|^2 [\delta f_{\mathbf{p}} [(1-n_{\mathbf{k}})n_{\mathbf{k}'}n_{\mathbf{p}'} + n_{\mathbf{k}}(1-n_{\mathbf{k}'})(1-n_{\mathbf{p}'})] - \delta f_{\mathbf{p}'} [(1-n_{\mathbf{k}})(1-n_{\mathbf{p}})n_{\mathbf{k}'} + n_{\mathbf{k}}n_{\mathbf{p}}(1-n_{\mathbf{k}'})]] \times \delta(\epsilon_{\mathbf{k}'} + \epsilon_{\mathbf{p}'} - \epsilon_{\mathbf{k}} - \epsilon_{\mathbf{p}}) \delta_{\mathbf{k}'+\mathbf{p}'-\mathbf{k}-\mathbf{p}}. \quad (17)$$

The corrections to the distribution functions can be presented in the form

$$\delta f_{\mathbf{k}} = \frac{\partial n_{\mathbf{k}}}{\partial \epsilon_{\mathbf{k}}} \varphi_{\mathbf{k}} = -\frac{\varphi_{\mathbf{k}}}{T} n_{\mathbf{k}}(1-n_{\mathbf{k}}),$$

$$\delta f_{\mathbf{p}} = \frac{\partial n_{\mathbf{p}}}{\partial \epsilon_{\mathbf{p}}} \varphi_{\mathbf{p}} = -\frac{\varphi_{\mathbf{p}}}{T} n_{\mathbf{p}}(1-n_{\mathbf{p}}). \quad (18)$$

However, it is important to take into account the following auxiliary relations:

$$\delta(\epsilon_{\mathbf{k}'} + \epsilon_{\mathbf{p}'} - \epsilon_{\mathbf{k}} - \epsilon_{\mathbf{p}}) = \int d\omega \delta(\epsilon_{\mathbf{k}'} - \epsilon_{\mathbf{k}} - \omega) \delta(\epsilon_{\mathbf{p}'} - \epsilon_{\mathbf{p}} + \omega),$$

$$\delta_{\mathbf{k}'+\mathbf{p}'-\mathbf{k}-\mathbf{p}} = \sum_{\mathbf{q}} \delta_{\mathbf{k}'-\mathbf{k}-\mathbf{q}} \delta_{\mathbf{p}'-\mathbf{p}+\mathbf{q}}, \quad (1-n_{\mathbf{p}})n_{\mathbf{p}'} = N_{-\omega}(n_{\mathbf{p}} - n_{\mathbf{p}'}), \quad (1+N_{\omega})(n_{\mathbf{p}} - n_{\mathbf{p}'}),$$

$$(1-n_{\mathbf{k}})n_{\mathbf{k}'} = N_{\omega}(n_{\mathbf{k}} - n_{\mathbf{k}'}), \quad N_{\omega} = \frac{1}{e^{\omega/T} - 1}, \quad \frac{\partial N}{\partial \omega} = \frac{N_{-\omega}N_{\omega}}{T} = -\frac{N_{\omega}(1+N_{\omega})}{T}. \quad (19)$$

After some algebra, Eqs. (18) and (19) can be presented in the form

$$(\mathbf{F}, \mathbf{v}_{\mathbf{k}}) \frac{\partial n_{\mathbf{k}}}{\partial \epsilon_{\mathbf{k}}} = 2\pi \sum_{\mathbf{p}', \mathbf{k}', \mathbf{p}, \mathbf{q}} \int d\omega |U_{\mathbf{p}'-\mathbf{p}}|^2 (\varphi_{\mathbf{k}} - \varphi_{\mathbf{k}'}) \frac{\partial N}{\partial \omega} (n_{\mathbf{p}} - n_{\mathbf{p}'}) (n_{\mathbf{k}} - n_{\mathbf{k}'}) \delta(\epsilon_{\mathbf{k}'} - \epsilon_{\mathbf{k}} - \omega) \delta(\epsilon_{\mathbf{p}'} - \epsilon_{\mathbf{p}} + \omega) \delta_{\mathbf{k}'-\mathbf{k}-\mathbf{q}} \delta_{\mathbf{p}'-\mathbf{p}+\mathbf{q}},$$

$$(\mathbf{F}, \mathbf{v}_{\mathbf{p}}) \frac{\partial n_{\mathbf{p}}}{\partial \epsilon_{\mathbf{p}}} = 2\pi \sum_{\mathbf{p}', \mathbf{k}', \mathbf{k}, \mathbf{q}} \int d\omega |U_{\mathbf{p}'-\mathbf{p}}|^2 (\varphi_{\mathbf{p}} - \varphi_{\mathbf{p}'}) \frac{\partial N}{\partial \omega} (n_{\mathbf{p}} - n_{\mathbf{p}'}) (n_{\mathbf{k}} - n_{\mathbf{k}'}) \delta(\epsilon_{\mathbf{k}'} - \epsilon_{\mathbf{k}} - \omega) \delta(\epsilon_{\mathbf{p}'} - \epsilon_{\mathbf{p}} + \omega) \delta_{\mathbf{k}'-\mathbf{k}-\mathbf{q}} \delta_{\mathbf{p}'-\mathbf{p}+\mathbf{q}}. \quad (20)$$

The energy transferred between colliding holes ω is of the order of temperature, $\omega \sim T$. Thus, in degenerate case the difference of distribution functions can be expanded as

$$n_{\mathbf{k}} - n_{\mathbf{k}'} = n(\epsilon_{\mathbf{k}}) - n(\epsilon_{\mathbf{k}} + \omega) \approx -\omega \frac{\partial n_{\mathbf{k}}}{\partial \epsilon_{\mathbf{k}}}, \quad n_{\mathbf{p}} - n_{\mathbf{p}'} = n(\epsilon_{\mathbf{p}}) - n(\epsilon_{\mathbf{p}} - \omega) \approx \omega \frac{\partial n_{\mathbf{p}}}{\partial \epsilon_{\mathbf{p}}}. \quad (21)$$

Referring to Eq. (21), the derivative $\frac{\partial n_{\mathbf{k}}}{\partial \epsilon_{\mathbf{k}}}$ represents the rate of change of the occupation number $n_{\mathbf{k}}$ with respect to the energy $\epsilon_{\mathbf{k}}$. It captures the effects and contributions of various scattering processes, including both elastic and inelastic scattering, determining the thermal and transport properties, respectively. Substituting Eq. (20) into Eqs. (21),

one finds

$$\begin{aligned}(\mathbf{F}, \mathbf{v}_\mathbf{k}) &= -2\pi \sum_{\mathbf{p}, \mathbf{q}} |U_\mathbf{q}|^2 (\varphi_\mathbf{k} - \varphi_{\mathbf{k}+\mathbf{q}}) \frac{\partial n_\mathbf{p}}{\partial \epsilon_\mathbf{p}} \int \omega^2 d\omega \frac{\partial N}{\partial \omega} \delta(\epsilon_{\mathbf{k}+\mathbf{q}} - \epsilon_\mathbf{k} - \omega) \delta(\epsilon_{\mathbf{p}-\mathbf{q}} - \epsilon_\mathbf{p} + \omega), \\ (\mathbf{F}, \mathbf{v}_\mathbf{p}) &= -2\pi \sum_{\mathbf{k}, \mathbf{q}} |U_\mathbf{q}|^2 (\varphi_\mathbf{p} - \varphi_{\mathbf{p}-\mathbf{q}}) \frac{\partial n_\mathbf{k}}{\partial \epsilon_\mathbf{k}} \int \omega^2 d\omega \frac{\partial N}{\partial \omega} \delta(\epsilon_{\mathbf{k}+\mathbf{q}} - \epsilon_\mathbf{k} - \omega) \delta(\epsilon_{\mathbf{p}-\mathbf{q}} - \epsilon_\mathbf{p} + \omega).\end{aligned}\quad (22)$$

Due to the degeneracy of both types of holes, one can determine $|\mathbf{k}|$ from the dispersion relation (assuming isotropic $\partial n_\mathbf{k}/\partial \epsilon_\mathbf{k}$): $|\mathbf{k}| = k_0$, where k_0 corresponds to the Fermi surface defined by $v k_0 = \mu$. Similarly, we can determine $|\mathbf{p}| = p_0$ from $p_0^2/2m + \Delta = \mu$ by considering the partial derivative $\partial n_\mathbf{p}/\partial \epsilon_\mathbf{p}$.

Let us also introduce the distribution functions corrections $\varphi_\mathbf{k}$ in the form $\varphi_\mathbf{k} = (\mathbf{F}, \mathbf{v}_\mathbf{k}) \chi(\epsilon_\mathbf{k})$, where $\chi(\epsilon_\mathbf{k})$ is an arbitrary function of energy. For degenerate hole gases, the function $\chi(\epsilon_\mathbf{k})$ can be considered as a constant, $\chi(\epsilon_\mathbf{k}) \equiv \chi_0 \equiv \tau$. Consequently, we have the following expressions:

$$\begin{aligned}(\mathbf{F}, \mathbf{v}_\mathbf{k}) &= 2\pi \tau_{dh} \sum_{\mathbf{p}, \mathbf{q}} |U_\mathbf{q}|^2 (\mathbf{F}, (\mathbf{v}_\mathbf{k} - \mathbf{v}_{\mathbf{k}+\mathbf{q}})) \frac{\partial n_\mathbf{p}}{\partial \epsilon_\mathbf{p}} \int \omega^2 d\omega \frac{\partial N}{\partial \omega} \delta(\epsilon_{\mathbf{k}+\mathbf{q}} - \epsilon_\mathbf{k} - \omega) \delta(\epsilon_{\mathbf{p}-\mathbf{q}} - \epsilon_\mathbf{p} + \omega), \\ (\mathbf{F}, \mathbf{v}_\mathbf{p}) &= 2\pi \tau_{hd} \sum_{\mathbf{k}, \mathbf{q}} |U_\mathbf{q}|^2 (\mathbf{F}, (\mathbf{v}_\mathbf{p} - \mathbf{v}_{\mathbf{p}-\mathbf{q}})) \frac{\partial n_\mathbf{k}}{\partial \epsilon_\mathbf{k}} \int \omega^2 d\omega \frac{\partial N}{\partial \omega} \delta(\epsilon_{\mathbf{k}+\mathbf{q}} - \epsilon_\mathbf{k} - \omega) \delta(\epsilon_{\mathbf{p}-\mathbf{q}} - \epsilon_\mathbf{p} + \omega),\end{aligned}\quad (23)$$

where τ_{dh} is an Dirac holes scattering time off the heavy holes, whereas τ_{hd} describes the scattering of heavy holes off the Dirac ones. In the limit of small wave vectors \mathbf{q} , the expressions entering into above expressions can be approximated as

$$\mathbf{F} \cdot (\mathbf{v}_\mathbf{k} - \mathbf{v}_{\mathbf{k}+\mathbf{q}}) = v \mathbf{F} \cdot \left(\frac{\mathbf{k}}{k} - \frac{\mathbf{k} + \mathbf{q}}{|\mathbf{k} + \mathbf{q}|} \right) \approx v \frac{(\mathbf{F}, \mathbf{k})(\mathbf{q}, \mathbf{k}) - (\mathbf{F}, \mathbf{q})k^2}{k^3} + v \frac{(\mathbf{F}, \mathbf{k})[q^2 k^2 - 3(\mathbf{q}, \mathbf{k})^2] + 2k^2(\mathbf{F}, \mathbf{q})(\mathbf{q}, \mathbf{k})}{2k^5}, \quad (24)$$

for the Dirac holes, and

$$\mathbf{F} \cdot (\mathbf{v}_\mathbf{p} - \mathbf{v}_{\mathbf{p}-\mathbf{q}}) = \frac{(\mathbf{F}, \mathbf{q})}{m}, \quad (25)$$

for heavy ones. Expanding for small momentum transfer also in Delta functions, we get

$$\begin{aligned}v \frac{(\mathbf{F}, \mathbf{k})}{k} &= 2\pi \tau_{dh} \sum_{\mathbf{p}, \mathbf{q}} |U_\mathbf{q}|^2 v \left[\frac{(\mathbf{F}, \mathbf{k})(\mathbf{q}, \mathbf{k}) - (\mathbf{F}, \mathbf{q})k^2}{k^3} + \frac{(\mathbf{F}, \mathbf{k})[q^2 k^2 - 3(\mathbf{q}, \mathbf{k})^2] + 2k^2(\mathbf{F}, \mathbf{q})(\mathbf{q}, \mathbf{k})}{2k^5} \right] \\ &\quad \times \frac{\partial n_\mathbf{p}}{\partial \epsilon_\mathbf{p}} \int \omega^2 d\omega \frac{\partial N}{\partial \omega} \delta\left(v \frac{\mathbf{qk}}{k} - \omega\right) \delta\left(-\frac{\mathbf{pq}}{m} + \omega\right), \\ \frac{(\mathbf{F}, \mathbf{p})}{m} &= 2\pi \tau_{hd} \sum_{\mathbf{k}, \mathbf{q}} |U_\mathbf{q}|^2 \frac{(\mathbf{F}, \mathbf{q})}{m} \frac{\partial n_\mathbf{k}}{\partial \epsilon_\mathbf{k}} \int \omega^2 d\omega \frac{\partial N}{\partial \omega} \delta\left(v \frac{\mathbf{qk}}{k} - \omega\right) \delta\left(-\frac{\mathbf{pq}}{m} + \omega + q^2/2m\right).\end{aligned}\quad (26)$$

Integrating over the angles, we get

$$\begin{aligned}\frac{1}{\tau_{dh}} &= \frac{4\pi}{(2\pi)^4 (k_0 v)^2} \int q dq |U_\mathbf{q}|^2 \int \omega^2 d\omega \frac{\partial N}{\partial \omega} \int p dp \frac{\partial n_\mathbf{p}}{\partial \epsilon_\mathbf{p}} \frac{\sqrt{(vq)^2 - \omega^2}}{\sqrt{(v_p q)^2 - \omega^2}}, \\ \frac{1}{\tau_{hd}} &= \frac{4\pi}{(2\pi)^4 p^2} \int q dq |U_\mathbf{q}|^2 \int \omega^2 d\omega \frac{\partial N}{\partial \omega} \frac{q^2}{\sqrt{(v_p q)^2 - (\omega + q^2/2m)^2} \sqrt{(vq)^2 - \omega^2}} \int k dk \frac{\partial n_\mathbf{k}}{\partial \epsilon_\mathbf{k}},\end{aligned}\quad (27)$$

where $v_p = p/m_h$. These expressions hold for any type of hole statistics. Below we consider two cases: when Dirac holes are always degenerate, whereas the heavy one are either degenerate or nondegenerate.

A. Degenerate Dirac and heavy holes

At low temperatures and high hole densities, when a Fermi energy is located above Δ , one has $\partial n_\mathbf{p}/\partial \epsilon_\mathbf{p} = -\delta(\Delta + \epsilon_\mathbf{p} - \mu)$ and $\partial n_\mathbf{k}/\partial \epsilon_\mathbf{k} = -\delta(vk - \mu)$. Thus, the relation $v_{p=p_0} =$

$v_F = p_0/m$ represents the Fermi velocity of heavy holes, which is a characteristic velocity for fermionic particles. Finally, ignoring the ω dependence in square roots in Eqs. (27), and taking into account that $\int p dp \frac{\partial n_\mathbf{p}}{\partial \epsilon_\mathbf{p}} = -m$, $\int k dk \frac{\partial n_\mathbf{k}}{\partial \epsilon_\mathbf{k}} =$

$= -\mu/v^2$, one finds

$$\frac{1}{\tau_{dh}} = -\frac{4\pi m}{(2\pi)^4(vk_0)(v_F k_0)} \left(\int q dq |U_q|^2 \right) \left(\int \omega^2 d\omega \frac{\partial N}{\partial \omega} \right),$$

$$\frac{1}{\tau_{hd}} = -\frac{4\pi \mu/v^2}{(2\pi)^4(vp_0)(v_F p_0)} \left(\int q dq |U_q|^2 \right) \left(\int \omega^2 d\omega \frac{\partial N}{\partial \omega} \right). \quad (28)$$

A model of contact interhole interaction. Here, we analyze the contact interaction model assuming that $U_q = U_0$. Integrating as

$$\int q dq |U_q|^2 = |U_0|^2 \int_0^{2\min(k_0, p_0)} q dq = 2|U_0|^2 (\min(k_0, p_0))^2,$$

$$\int_{-\infty}^{\infty} \omega^2 d\omega \frac{\partial N}{\partial \omega} = -\frac{2\pi^2 T^2}{3}, \quad (29)$$

we find (recovering Plank and Boltzmann constants)

$$\frac{1}{\tau_{dh}} = A \frac{m_h(kT)^2 |U_0|^2}{3\pi \hbar^5 v v_F} \sim T^2,$$

$$\frac{1}{\tau_{hd}} = \frac{(\mu/v^2)(kT)^2 |U_0|^2 k_0^2}{3\pi \hbar^5 v v_F p_0^2} \sim T^2. \quad (30)$$

These formulas are applicable in the framework of QFT. Here k_0 is defined as $vk_0 = \mu$, $p_0 = m_h v_F = \sqrt{2m_h(\mu - \Delta)}$ for degenerate Dirac and heavy holes gases. It should be noted that the expressions (30) satisfy the relation $m_d n_d / \tau_{dh} = m_h n_h / \tau_{hd}$, where $m_d = \mu/v^2$, $4\pi n_d = k_0^2$, and $4\pi n_h = p_0^2$. The latter expressions hold for degenerate electron gas. A represents a numerical coefficient that varies based on the specifics of the Coulomb interactions.

The contact interaction parameter U_0 can be estimated as overscreened Coulomb interaction, $U_0 = 2\pi e^2 / q_s$, where q_s is a screening wave vector. It is worth noting that this prescription applies to strongly degenerate Fermi liquids. Assuming that the main contribution to the screening is determined by the heavy holes due to its high density of states, the screening wave vector can be written as $q_s = m_h e^2 / (\epsilon \hbar^2)$, where ϵ is the dielectric constant of the material.

Figure 4 illustrates the relationship between the relaxation rate $1/\tau_{dh}$ and $1/\tau_{hd}$ and temperature. The values are computed using Eqs. (30) with parameter $A = 1$. It is evident that this relationship adheres to a quadratic function of temperature T^2 . One can see that $1/\tau_{dh} > 1/\tau_{hd}$.

B. Degenerate Dirac and nondegenerate heavy holes

At low densities and moderately high temperatures, the heavy holes become nondegenerate. In this case the distribution function of heavy holes reads

$$n_p = \frac{2\pi \hbar^2 n_h}{m_h T} \exp\left(-\frac{\epsilon_p}{kT}\right). \quad (31)$$

Calculations similar to the presented above yield

$$\frac{1}{\tau_{dh}^*} = B \frac{1.7(kT)^2 |U_0|^2 n_h m_h}{\hbar^3 k_0^2 v v_T} \sim T^{7/2},$$

$$\frac{1}{\tau_{hd}^*} = \frac{(kT)^2 |U_0|^2 n_d m_d}{\hbar^3 k_0^2 v v_T} \sim T^{7/2}. \quad (32)$$

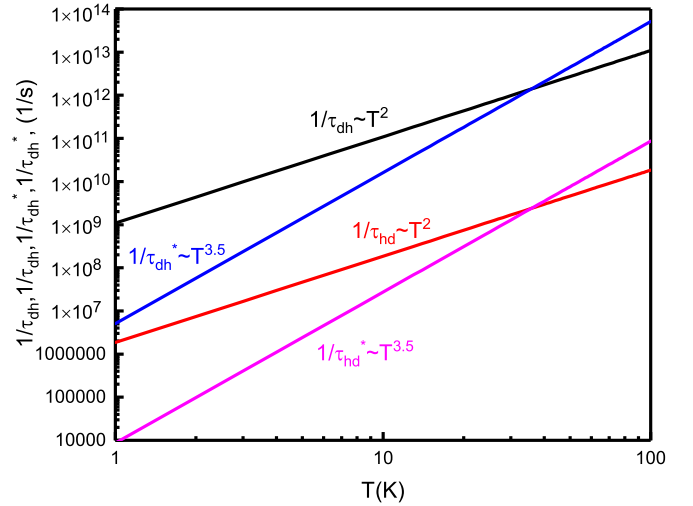


FIG. 4. Temperature dependence of the relaxation rate. The lines are computed using equations (30) (black), (30) (red), (32) (blue), and (32) (magenta).

The density of Dirac holes is $4\pi n_d = k_0^2 = 4\pi \mu^2 / v^2 = m_d \mu$, $v_T = \sqrt{2kT/m}$. The expressions for relaxation times, Eq. (32) also satisfy the general relation $m_d n_d / \tau_{dh} = m_h n_h / \tau_{hd}$. B is a numerical coefficient as a parameter A , contingent upon the nature of Coulomb interactions.

The contact interaction parameter U_0 here can also be estimated as overscreened Coulomb interaction, $U_0 = 2\pi e^2 / q_T$, where q_T is a screening wave vector. Assuming again that the main contribution to the screening is determined by the nondegenerate heavy holes due to its high density of states, the screening wave vector can be written now as $q_T = 2\pi e^2 n_h / \epsilon kT$, where ϵ is the dielectric constant of the material.

Figure 4 illustrates the relationship between the relaxation rates $1/\tau_{dh}^*$ and $1/\tau_{hd}^*$ and temperature, represented by blue and magenta lines. The computations are carried out utilizing Eqs. (32) with the parameter B set to 0.6. Clearly, across a broad temperature range, the interaction rate maintains the relationship $1/\tau_{dh}^* > 1/\tau_{hd}^*$ for both regimes. Furthermore, the relaxation rate $1/\tau_{hd}^*$ surpasses $1/\tau_{dh}^*$ at temperatures exceeding 40 K.

VII. COMPARISON WITH THE EXPERIMENT

In Secs. V and VI we provide a theoretical description of a 2D system with two types of carriers, one with a linear and another with a quadratic spectrum. The rate of the momentum transfer between these two types of carriers is found. We consider a fully Fermi degenerate regime (FD) for both systems at low temperatures ($kT < \mu - \Delta$) and a partially degenerate regime (PD), when the Dirac particles remain degenerate, while the heavy holes obey the Boltzmann statistics ($\mu - \Delta < kT < \mu$).

In a fully degenerate (FD) regime we obtain the conventional expression for the particle-particle collisions, slightly modified due to the difference in spectrum and is given by Eqs. (30). Note that $1/\tau_{hd} \ll 1/\tau_{dh}$, and conventional T^2 behavior for $1/\tau_{int} \sim 1/\tau_{dh}$, characteristic of a particle with parabolic dispersion, becomes apparent.

TABLE II. Fitting parameters in Eqs. (1)–(5) for three samples.

Sample	τ_h	τ_d	n_h	n_d	A	B
	10^{-13}	10^{-13}	10^{11}	10^{11}		
	s	s	cm^{-2}	cm^{-2}		
A	1.7	12.2	4.78	0.21	1.2	0.5
B	0.94	8.5	4.53	0.22	1.8	0.6
C	1.2	10.7	5.52	0.23	1.4	0.6
A	2.3	3	0.28	0.17		0.15
B	1.8	3.5	0.53	0.16		0.15
C	2.7	3.55	0.28	0.16		0.16

In a partially degenerate (PD) regime ($\mu - \Delta < kT < \mu$), the particle-particle collision rate $1/\tau_{dh,hd}^*$ shows a distinct temperature dependence. By adjusting expression for scattering rate while considering the constraint that interactions between holes conserve the overall momentum density it is given by Eqs. (32). Because $1/\tau_{int}^* = 1/\tau_{dh}^* + 1/\tau_{hd}^* \sim 1/\tau_{dh}^*$, it is expected that the temperature-dependent behavior of the relaxation rate can be described as follows: $1/\tau_{int}^* \sim T^{3.5}$. In Fig. 3 we compare the results of the calculations with experimental $\rho(T)$ dependencies using Eqs. (9) and (30) for high and low total densities, corresponding to the different regimes, denoted as FD and PD regimes within corresponding models. We plot the experimentally measured excess resistivity and that obtained theoretically $\Delta\rho(T)$ for three samples. For comparison with the theory we conducted a fitting analysis of the temperature-dependent data, as depicted in Fig. 3, using a single adjustable parameters denoted as A and B. These parameters account for the strength of interaction between the Dirac and heavy holes, as described in Eqs. (9) and (32). The scattering parameters, denoted as $\tau_{h(d)}$, predominantly dictate the resistivity at lower temperatures. Importantly, adjusting these parameters within a reasonable range does not affect the friction coefficient, which is the key factor responsible for the temperature dependence of resistivity. In Figs. 3(a)–3(c) we plot theoretical dependencies of the resistivity excess for high total density ($N_h \approx 5 \times 10^{11} \text{ cm}^{-2}$). Experimental data closely follows the expected dependence $\Delta\rho(T) \sim T^2$ for parameters indicated in Table II.

In Figs. 3(d)–3(f) we also plot theoretical dependencies of the resistivity excess for low total density ($N_h \approx 0.5 \times 10^{11} \text{ cm}^{-2}$) using the PD model, which is in agreement with experimental data. Corresponding parameters are shown in the Table I. It is important to emphasize that the expected behavior of $1/\tau_{dh}$ follows a power-law relationship with temperature $\sim T^{3.5}$, while resistivity exhibits a temperature-dependent relationship described by a power law of $\sim T^\alpha$ ($\alpha \approx 3$). This difference arises because resistivity demonstrates a saturation effect at low temperatures, attributed to scattering by impurities, and at high temperatures, it is influenced by various parameters, including the effective mass ratio as described in Eq. (1), leading to a temperature dependence resembling $\sim T^3$.

In Fig. 5, we illustrate the variation of the ratio $\rho(50 \text{ K})/\rho(4.2 \text{ K})$ with respect to the total density N_h across various values of the scattering relaxation time ratio τ_d/τ_h , calculated from Eqs. (9) and (32). Notably, one observes that

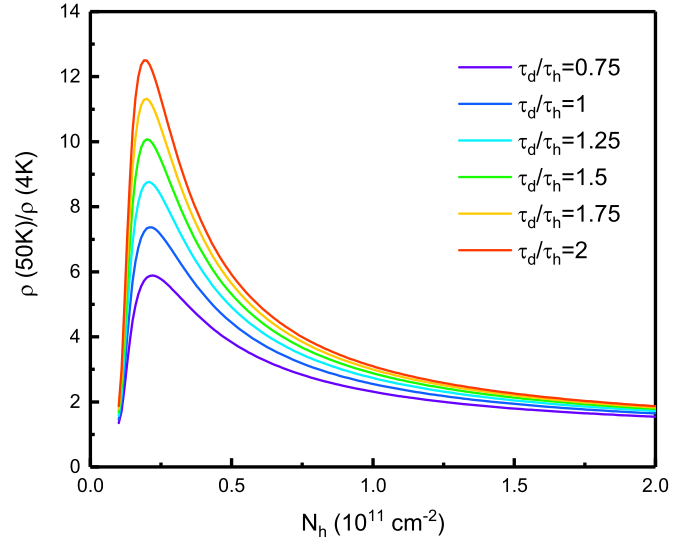


FIG. 5. Ratio of resistivity at low- and high-temperature limits $\frac{\rho(T=50\text{K})}{\rho(T=4.2\text{K})}$ as a function of the density N_h for different ratio τ_d/τ_h , calculated from Eqs. (9) and (32). Parameters are $\tau_d = 3 \times 10^{-13} \text{ s}$, $B = 0.15$.

in realistic samples, this ratio converges towards the range 6–12. This observation underscores a unique scenario in the realm of solid-state physics, wherein resistance is predominantly governed by interactions between particles. In stark contrast to the more typical scenarios where resistance is primarily influenced by disorder or phonon scattering, here, particle-particle collisions play a pivotal role, significantly exceeding the impact of impurity-related scattering. At higher total densities and temperatures exceeding 30 K, heavy holes enter into the Boltzmann regime, leading to an expected alteration in resistivity with changing temperature regimes. To verify this, we conducted a comparison between experimental data and calculations using the PD model. The outcomes of this comparison are illustrated in Figs. 3(a)–3(c). Notably, there exists a reasonable concordance with the PD model. However, owing to the limited temperature range, it proves challenging to experimentally discern between these two regimes at such densities. The variation in parameter B between high and low densities can be attributed to a deficiency in the model of short-range potential when it approaches the limit of the actual Coulomb potential.

One can see that the sample B seems to deviate from theoretical model at low temperatures [Fig. 3(e)]. We attribute this deviation to density inhomogeneity, which may render our model less applicable at lower temperatures. However, it is noteworthy that at elevated temperatures, the dependence aligns with a T^3 relationship across a range exceeding one order of magnitude. Notably, we observe a T^3 dependence in samples A and C that adheres to this trend across more than three orders of magnitude, an occurrence not commonly observed in experiments.

VIII. CONCLUSIONS

In conclusion, our investigation focused on the temperature-dependent resistivity in a gapless HgTe quantum

well. We observed quadratic temperature dependencies arising from interactions between the Dirac and heavy holes in the fully degenerate regime. Conversely, a cubic temperature dependence emerged when heavy holes conformed to Boltzmann statistics while the Dirac holes retained Fermi liquid characteristics.

To validate our findings, we compared theoretical predictions with experimental data, revealing a satisfactory agreement. An interesting observation is that within the temperature range 10–100 K, hole-hole scattering proves to be significantly more influential than impurity scattering. This is an uncommon occurrence, as in conventional metallic

systems, particle-particle collisions typically do not limit conductivity.

ACKNOWLEDGMENTS

This work is supported by FAPESP (São Paulo Research Foundation) Grants No. 2019/16736-2 and No. 2021/12470-8, CNPq (National Council for Scientific and Technological Development), and by the Ministry of Science and Higher Education of the Russian Federation and Foundation for the Advancement of Theoretical Physics and Mathematics “BASIS.”

-
- [1] R. N. Gurzhi, Minimum of resistance in impurity-free conductors, *Sov. Phys. JETP* **44**, 771 (1963) [*Sov. Phys. Usp.* **11**, 255 (1968)].
- [2] M. Polini and A. K. Geim, Viscous electron fluids, *Phys. Today* **73**, 28 (2020).
- [3] B. N. Narozhny, Hydrodynamic approach to two-dimensional electron systems, *La Rivista del Nuovo Cimento* **45**, 661 (2022).
- [4] M. J. M. de Jong and L. W. Molenkamp, Hydrodynamic electron flow in high-mobility wires, *Phys. Rev. B* **51**, 13389 (1995).
- [5] G. M. Gusev, A. D. Levin, E. V. Levinson, and A. K. Bakarov, Viscous electron flow in mesoscopic two-dimensional electron gas, *AIP Adv.* **8**, 025318 (2018).
- [6] G. M. Gusev, A. D. Levin, E. V. Levinson, and A. K. Bakarov, Viscous transport and Hall viscosity in a two-dimensional electron system, *Phys. Rev. B* **98**, 161303(R) (2018).
- [7] G. M. Gusev, A. S. Jaroshevich, A. D. Levin, Z. D. Kvon, and A. K. Bakarov, Stokes flow around an obstacle in viscous two-dimensional electron liquid, *Sci. Rep.* **10**, 7860 (2020).
- [8] G. M. Gusev, A. S. Jaroshevich, A. D. Levin, Z. D. Kvon, and A. K. Bakarov, Viscous magnetotransport and Gurzhi effect in bilayer electron system, *Phys. Rev. B* **103**, 075303 (2021).
- [9] R. Krishna Kumar, D. A. Bandurin, F. M. D. Pellegrino, Y. Cao, A. Principi, H. Guo, G. H. Auton, M. Ben Shalom, L. A. Ponomarenko, G. Falkovich *et al.*, Superballistic flow of viscous electron fluid through graphene constrictions, *Nat. Phys.* **13**, 1182 (2017).
- [10] E. H. Hwang and S. Das Sarma, Temperature dependent resistivity of spin-split subbands in GaAs two-dimensional hole systems, *Phys. Rev. B* **67**, 115316 (2003).
- [11] K. E. Nagaev and A. A. Manoshin, Electron-electron scattering and transport properties of spin-orbit coupled electron gas, *Phys. Rev. B* **102**, 155411 (2020).
- [12] K. E. Nagaev, Electron-electron scattering and conductivity of disordered systems with a Galilean-invariant spectrum, *Phys. Rev. B* **106**, 085411 (2022).
- [13] E. B. Olshanetsky, Z. D. Kvon, M. V. Entin, L. I. Magarill, N. N. Mikhailov, and S. A. Dvoretzky, Scattering processes in a two-dimensional semimetal, *JETP Lett.* **89**, 290 (2009).
- [14] M. V. Entin, L. I. Magarill, E. B. Olshanetsky, Z. D. Kvon, N. N. Mikhailov, and S. A. Dvoretzky, The effect of electron-hole scattering on transport properties of a 2D semimetal in the HgTe quantum well, *J. Exp. Theor. Phys.* **117**, 933 (2013).
- [15] Y. Nam, D.-K. Ki, D. Soler-Delgado, and A. F. Morpurgo, Electron-hole collision limited transport in charge-neutral bilayer graphene, *Nat. Phys.* **13**, 1207 (2017).
- [16] C. Tan, D. Y. H. Ho, L. Wang, J. I. A. Li, I. Yudhistira, D. A. Rhodes, T. Taniguchi, K. Watanabe, K. Shepard, P. L. McEuen *et al.*, Dissipation-enabled hydrodynamic conductivity in a tunable bandgap semiconductor, *Sci. Adv.* **8**, eabi8481 (2022).
- [17] D. A. Bandurin, A. Principi, I. Y. Phinney, T. Taniguchi, K. Watanabe, and P. Jarillo-Herrero, Interlayer electron-hole friction in tunable twisted bilayer graphene semimetal, *Phys. Rev. Lett.* **129**, 206802 (2022).
- [18] M. Lampe, Transport theory of the partially degenerate plasma, *Phys. Rev.* **174**, 276 (1968).
- [19] L. G. Gerchikov and A. V. Subashiev, Interface states in subband structure of semiconductor quantum wells, *Physica Status Solidi (b)* **160**, 443 (1990).
- [20] C. L. Kane and E. J. Mele, Z_2 topological order and the quantum spin Hall effect, *Phys. Rev. Lett.* **95**, 146802 (2005); Quantum spin Hall effect in graphene, **95**, 226801 (2005).
- [21] B. A. Bernevig and S. C. Zhang, Quantum spin Hall effect, *Phys. Rev. Lett.* **96**, 106802 (2006); B. A. Bernevig, T. L. Hughes, and S. C. Zhang, Quantum spin Hall effect and topological phase transition in HgTe quantum wells, *Science* **314**, 1757 (2006).
- [22] M. König, S. Wiedmann, C. Brüne, A. Roth, H. Buhmann, L. W. Molenkamp, X.-L. Qi, and S.-C. Zhang, Quantum spin Hall insulator state in HgTe quantum wells, *Science* **318**, 766 (2007).
- [23] G. M. Gusev, Z. D. Kvon, E. B. Olshanetsky, and N. N. Mikhailov, Mesoscopic transport in two-dimensional topological insulators, *Solid State Commun.* **302**, 113701 (2019).
- [24] B. Büttner, C. X. Liu, G. Tkachov, E. G. Novik, C. Brüne, H. Buhmann, E. M. Hankiewicz, P. Recher, B. Trauzettel, S. C. Zhang, and L. W. Molenkamp, Single valley Dirac fermions in zero-gap HgTe quantum wells, *Nat. Phys.* **7**, 418 (2011).
- [25] D. A. Kozlov, Z. D. Kvon, N. N. Mikhailov, and S. A. Dvoretzky, Weak localization of Dirac fermions in HgTe quantum wells, *JETP Lett.* **96**, 730 (2013).
- [26] G. M. Gusev, D. A. Kozlov, A. D. Levin, Z. D. Kvon, N. N. Mikhailov, and S. A. Dvoretzky, Robust helical edge transport at $\nu = 0$ quantum Hall state, *Phys. Rev. B* **96**, 045304 (2017).
- [27] S. S. Krishtopenko, W. Desrat, K. E. Spirin, C. Consejo, S. Ruffenach, F. Gonzalez-Posada, B. Jouault, W. Knap, K. V.

- Maremyanin, V. I. Gavrilenko, G. Boissier, J. Torres, M. Zaknourne, E. Tournié, and F. Teppe, Massless Dirac fermions in III-V semiconductor quantum wells, *Phys. Rev. B* **99**, 121405(R) (2019).
- [28] Z. D. Kvon, E. B. Olshanetsky, D. A. Kozlov, N. N. Mikhailov, and S. A. Dvoretzky, Two-dimensional electron-hole system in a HgTe-based quantum well, *JETP Lett.* **87**, 502 (2008).
- [29] A. Shuvaev, V. Dziom, J. Gospodaric, E. G. Novik, A. A. Dobretsova, N. N. Mikhailov, Z. D. Kvon, and A. Pimenov, Band structure near the Dirac point in HgTe quantum wells with critical thickness, *Nanomaterials* **12**, 2492 (2022).
- [30] G. M. Gusev, E. B. Olshanetsky, F. G. G. Hernandez, O. E. Raichev, N. N. Mikhailov, and S. A. Dvoretzky, Two-dimensional topological insulator state in double HgTe quantum well, *Phys. Rev. B* **101**, 241302(R) (2020).
- [31] G. M. Gusev, Z. D. Kvon, D. A. Kozlov, E. B. Olshanetsky, M. V. Entin, and N. N. Mikhailov, Transport through the network of topological channels in HgTe based quantum well, *2D Mater.* **9**, 015021 (2022).
- [32] N. N. Mikhailov, R. N. Smirnov, S. A. Dvoretzky, Yu. G. Sidorov, V. A. Shvets, E. V. Spesivtsev, and S. V. Rykhlitski, Growth of Hg_{1-x}Cd_xTe nanostructures by molecular beam epitaxy with ellipsometric control, *Intl. J. Nanotech.* **3**, 120 (2006).
- [33] Y. O. Melezhik, J. V. Gumenjuk-Sichevska, and F. F. Sizov, Electron relaxation and mobility in the inverted band quantum well CdTe/Hg_{1-x}Cd_xTe/CdTe, *Semicond. Phys. Quantum Electron. Optoelectron.* **17**, 85 (2014).
- [34] H. K. Pal, V. I. Yudson, and D. L. Maslov, Resistivity of non Galilean invariant term Fermi and non Fermi liquids, *Lith. J. Phys.* **52**, 142 (2012).
- [35] J. Appel and A. W. Overhauser, Cyclotron resonance in two interacting electron systems with application to Si inversion layers, *Phys. Rev. B* **18**, 758 (1978).
- [36] S. S. Murzin, S. I. Dorozhkin, G. Landwehr, and A. C. Gossard, Effect of hole-hole scattering on the conductivity of the two-component 2D hole gas in GaAs/(AlGa)As heterostructures, *JETP Lett.* **67**, 113 (1998).
- [37] V. Kravchenko, N. Minina, A. Savino, P. Hansen, C. B. Sorensen, and W. Kraak, Positive magnetoresistance and hole-hole scattering in GaAs/Al_{0.5}Ga_{0.5}As heterostructures under uniaxial compression, *Phys. Rev. B* **59**, 2376 (1999).
- [38] J. P. Laurenti, J. Camasse, A. Bouhemadou, B. Toulouse, R. Legros, and A. Lussion, Temperature dependence of the fundamental absorption edge of mercury cadmium telluride, *J. Appl. Phys.* **67**, 6454 (1990).
- [39] C. R. Becker, V. Latussek, A. Pfeuffer-Jeschke, G. Landwehr, and L. W. Molenkamp, Band structure and its temperature dependence for type-III HgTe/Hg_{1-x}Cd_xTe superlattices and their semimetal constituent, *Phys. Rev. B* **62**, 10353 (2000).
- [40] J. Li and K. Chang, Electric field driven quantum phase transition between band insulator and topological insulator, *Appl. Phys. Lett.* **95**, 222110 (2009).
- [41] T. Khouri, M. Bendias, P. Leubner, C. Brüne, H. Buhmann, L. W. Molenkamp, U. Zeitler, N. E. Hussey, and S. Wiedmann, High-temperature quantum Hall effect in finite gapped HgTe quantum wells, *Phys. Rev. B* **93**, 125308 (2016).
- [42] D. A. Kozlov, Z. D. Kvon, N. N. Mikhailov, S. A. Dvoretzky, S. Weishäupl, Y. Krupko, and J.-C. Portal, Quantum Hall effect in HgTe quantum wells at nitrogen temperatures, *Appl. Phys. Lett.* **105**, 132102 (2014).
- [43] S. S. Krishtopenko, I. Yahniuk, D. B. But, V. I. Gavrilenko, W. Knap, and F. Teppe, Pressure- and temperature-driven phase transitions in HgTe quantum wells, *Phys. Rev. B* **94**, 245402 (2016).